Appl. Phys. B 72, 109–113 (2001) / Digital Object Identifier (DOI) 10.1007/s003400000451

Applied Physics B
Lasers
and Optics

The focus of light – theoretical calculation and experimental tomographic reconstruction

S. Quabis, R. Dorn, M. Eberler, O. Glöckl, G. Leuchs*

Physics Department, Chair for Optics, University Erlangen–Nürnberg, Staudtstr. 7/B2, 91058 Erlangen, Germany
(E-mail: leuchs@physik.uni-erlangen.de)

Received: 14 July 2000/Published online: 30 November 2000 –

Abstract. We present numerical calculations on the field distribution in the focus of an optical system with high numerical aperture. The diffraction integrals which are based on the Debye approximation are derived and evaluated for a radially polarized input field with a doughnut-shaped intensity distribution. It is shown that this mode focusses down to a spot size significantly smaller as compared to the case of linear polarization. An experimental setup to measure the three-dimensional intensity distribution in the focal region is presented, which is based on the knife-edge method and on tomographic reconstruction.

PACS: 42.15.Dp; 42.25.Ja; 42.30.Wb

For many applications smaller two-dimensional focal spot sizes improve the performance of an optical system. In the case of confocal microscopy it is also important to have knowledge about the third dimension of the focal field distribution.

In a theoretical approach, Richards and Wolf [1] have established a vectorial diffraction theory for systems with high numerical aperture. They found that the focus of a linearly polarized beam is asymmetrically deformed. This asymmetry is an effect due to the vector character of the electric field and was described in detail by Stamnes [2]. It has been shown that this asymmetry can be overcome when a radially polarized input field is used which best fits the symmetry of the focussing system [3]. In the focus a strong longitudinal field component with a narrow intensity distribution is formed. Furthermore, the focal spot size can be reduced compared to the case of a linearly polarized input field. We will derive the diffraction integrals for focussing such a field distribution.

The performance of an optical system is typically characterized by measuring the optical transfer function (OTF) or the intensity point spread function (PSF). In a confocal interference microscope, aberrations of the optical system can be evaluated by measuring the defocus signal [4]. Another approach would be to determine the focal field distribution. A scheme to directly measure the complex field distribution in the focus of a system with high numerical aperture was proposed. In an interferometric setup the use of small (fluorescent) beads and two shifted focal field distributions is suggested [5]. We present a different experimental setup, which is based on the knife-edge method [6] combined with tomographic reconstruction, and which allows one to determine the three-dimensional intensity distribution in the focus of optical systems with high numerical aperture.

*Corresponding author.

1 Vector diffraction theory – Debye approximation

For high numerical aperture systems where effects due to the vector character of the electric field become important, a vector diffraction theory is necessary. A plane wave incident on a focussing system is transformed into a converging spherical wave. The starting point of the approach is to expand this spherical wave into an angular spectrum of plane waves [1, 2]. For large Fresnel numbers, as in our case, the Debye approximation can be used to calculate this angular spectrum. Literally speaking, only those plane waves contribute to the field in the focus the propagation directions of which correspond to the geometric optical rays. In this approximation, diffraction effects due to the edge of the aperture are not considered. The field in the focus can be evaluated by superposing those plane waves, keeping track of the phase and the direction of polarization. This yields

$$\boldsymbol{E}(\boldsymbol{r}_2) = \frac{-\mathrm{i}}{2\pi} \iint\limits_{\Omega_1} \mathrm{d}k_x \mathrm{d}k_y \frac{\boldsymbol{A}(k_x, k_y)}{k_z} \exp[\mathrm{i}\boldsymbol{k}\cdot(\boldsymbol{r}_2 - \boldsymbol{r}_1)]. \qquad (1)$$

Evaluating the problem, following the analysis of Richards and Wolf [1] for a linearly polarized input field, it turns out that the focal field no longer shows rotational symmetry. This behavior can easily be understood in a ray-tracing picture (Fig. 2a). For light rays propagating in the plane which contains the optical axis and which is perpendicular to the direction of the polarization vector $\boldsymbol{p}_0$ of the linearly polarized incoming field, all electric-field vectors are parallel in the focus and add up perfectly. However, the situation is different in

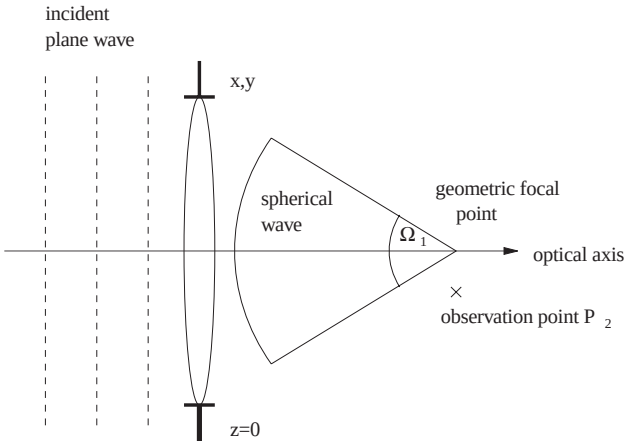

Fig. 1. An incoming plane wave is transformed into a spherical wave by the focussing system

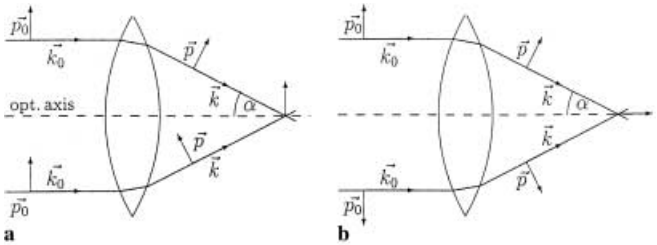

Fig. 2a,b. Ray-tracing model for focussing a linearly (**a**) and a radially (**b**) polarized incoming field

the plane which is perpendicular to the first plane, also containing the optical axis so that the direction of polarization is parallel to this plane, as is depicted in Fig. 2a. In this plane the electric-field vectors are not parallel in the image space, so that there is a partial cancellation of the field in the focus when the field components are superposed. As a result, lines of equal intensity in the focal plane are no longer circular.

However, for a polarization distribution with azimuthal symmetry, complete rotational symmetry of the field in the focus is expected. We now consider a radially polarized field. In the ray-tracing picture, for each plane containing the optical axis and the corresponding geometric optical ray, the electric-field vector is parallel to this plane (see Fig. 2b). Furthermore, for high numerical aperture systems, there exists a strong longitudinal field component parallel to the optical axis.

Such a radially polarized field distribution can be described as a superposition of a TEM_{10}-Gauss–Hermite mode with a polarization direction parallel to the x-axis and a TEM_{01} mode with a polarization direction parallel to the y-axis. The relative phase difference between the two modes has to be $\phi = 0$. Hence the field in the waist of this radially polarized doughnut mode is given by

$$\begin{aligned}\boldsymbol{E}(x,y) &= E_0\left(\exp\left[-\frac{\varrho^2}{\omega_0^2}\right]x\boldsymbol{e}_x + \exp\left[-\frac{\varrho^2}{\omega_0^2}\right]y\boldsymbol{e}_y\right)\\ &= E_0\exp\left[-\frac{\varrho^2}{\omega_0^2}\right]\varrho\boldsymbol{e}_\varrho, \end{aligned} \tag{2}$$

where $\varrho = \sqrt{x^2+y^2}$ and ω_0 denotes the beam radius.

We now derive, to our knowledge for the first time, the focal field distribution of this special, radially polarized input field. The results of this calculation have already been communicated in [3]. To proceed, we adapt the calculations described in [1, 2] to obtain the field for linear polarization. We start with (1) and have to determine the vector amplitude

$$\boldsymbol{A}(k_x,k_y) = \tilde{A}(k_x,k_y)\,\hat{p}_{\mathrm{rad}}(k_x,k_y)\,; \tag{3}$$

$\hat{p}_{\mathrm{rad}}$ indicates the direction of the electric field of each plane wave as given by geometric optics. Next, we introduce a set of spherical coordinates to rewrite the components of $\boldsymbol{k}$ and obtain

$$k_x = -k\sin\alpha\cos\beta \quad \text{and} \quad k_y = -k\sin\alpha\sin\beta\,. \tag{4}$$

Since the system is rotationally symmetric with respect to the optical axis, the factor $\tilde{A}$ depends only on α:

$$\tilde{A}(k_x,k_y) = A(\alpha)\,, \tag{5}$$

where α is the angle between $\boldsymbol{k}$ and the optical axis. For an aplanatic system, we obtain

$$A(\alpha) = E_0\, f\,\sin\alpha\exp\left(\frac{-(f\sin\alpha)^2}{\omega_0^2}\right)\sqrt{|\cos\alpha|}, \tag{6}$$

where we use the relation

$$A(\alpha) = A_0(f\sin\alpha)\sqrt{|\cos\alpha|}. \tag{7}$$

For the aplanatic system the distance from the optical axis in the aperture plane where the lens is situated is given by $\varrho = f\sin\alpha$. $A_0(\varrho)$ is the amplitude variation of the incident field as shown by Stamnes [2]. In our case $A_0(\varrho)$ is given by (2). The factor $\sqrt{|\cos\alpha|}$ accounts for energy conservation. $\hat{p}_{\mathrm{rad}}$ is a unit vector indicating the direction of the electric field:

$$\hat{p}_{\mathrm{rad}}(k_x(\alpha,\beta),k_y(\alpha,\beta)) = \begin{pmatrix}\cos(\alpha)\cos(\beta)\\ \cos(\alpha)\sin(\beta)\\ \sin(\alpha)\end{pmatrix}. \tag{8}$$

Rewriting (1) in terms of the coordinates α and β yields

$$\begin{aligned}\boldsymbol{E}(\tilde{r},\tilde{\theta},\tilde{\phi}) =& \frac{-\mathrm{i}k}{2\pi}\int_0^{2\pi}\mathrm{d}\beta\int_0^{\theta_1}\mathrm{d}\alpha A(\alpha)\sin\alpha\,\hat{p}_{\mathrm{rad}}(\alpha,\beta)\\ &\times\exp\{\mathrm{i}k\tilde{r}[\cos\tilde{\theta}\cos\alpha - \sin\tilde{\theta}\sin\alpha\cos(\beta-\tilde{\phi})]\}.\end{aligned} \tag{9}$$

The β-integration can be evaluated analytically using the relations

$$\int_0^{2\pi}\mathrm{d}\beta\cos(n\beta)\exp[\mathrm{i}t\cos(\beta-\gamma)] = 2\pi\mathrm{i}^n J_n(t)\cos(n\gamma), \tag{10}$$

$$\int_0^{2\pi}\mathrm{d}\beta\sin(n\beta)\exp[\mathrm{i}t\cos(\beta-\gamma)] = 2\pi\mathrm{i}^n J_n(t)\sin(n\gamma), \tag{11}$$

where n is an integer and $J_n(t)$ is the Bessel function of the first kind of the order n. Finally, we end up with the diffraction integral for a focussed radially polarized doughnut-

shaped input field, where we introduced cylindrical coordinates $(\tilde{\varrho}, \tilde{z}, \tilde{\phi})$ centered at the geometrical focus:

$$\boldsymbol{E}(\tilde{\varrho}, \tilde{z}, \tilde{\phi}) = -\frac{\mathrm{i}k}{2\pi} \int_0^{\theta_1} \mathrm{d}\alpha A(\alpha) \sin\alpha \exp(\mathrm{i}k\tilde{z}\cos\alpha) \times \begin{pmatrix} 2\pi\mathrm{i}\cos\alpha J_1(-k\tilde{\varrho}\sin\alpha)\cos\tilde{\phi} \\ 2\pi\mathrm{i}\cos\alpha J_1(-k\tilde{\varrho}\sin\alpha)\sin\tilde{\phi} \\ 2\pi\sin\alpha J_0(-k\tilde{\varrho}\sin\alpha) \end{pmatrix}, \quad (12)$$

with $\tilde{z} = \tilde{r}\cos\tilde{\theta}$ and $\tilde{\varrho} = \tilde{r}\sin\tilde{\theta}$. Thus, $\tilde{\varrho}$ describes the radial distance of the observation point from the optical axis, while $\tilde{z}$ is the distance of the observation point from the geometrical focus along the optical axis. Here, θ_1 is the maximum angle of incidence of the plane waves, and it is related to the numerical aperture of the system by $\sin\theta_1 = NA$.

2 Results of the numerical calculations

We have numerically evaluated the diffraction integrals in (12) as well as the formulae for a linearly polarized input field as described by Stamnes for various numerical apertures. We are interested in the time-averaged energy density of the electric field, that can be obtained from the electric field (in Gaussian units) with the relation

$$\langle w_{\mathrm{el}}(\tilde{\varrho}, \tilde{z}, \tilde{\phi})\rangle = \frac{1}{16\pi^2}\boldsymbol{E}\cdot\boldsymbol{E}^*. \quad (13)$$

For a linearly polarized input field, Fig. 3a shows that the intensity distribution in the focal plane no longer has rotational symmetry, although the intensity distribution of the initial field was rotationally symmetric. The figure shows the limit of high numerical apertures $NA \to 1.0$. The contour lines of equal intensity resemble more or less the shape of ellipses. In contrast, the energy density of the radially polarized field exhibits full rotational symmetry (Fig. 4a). Furthermore, evaluating the focal spot size shows that the focussed radially polarized beam has a slightly smaller area than the focussed linearly polarized field. The spot size is defined by the area enclosed by the contour line at half the maximum value. The spot sizes are $0.277\,\lambda^2$ and $0.266\,\lambda^2$ for the linearly polarized field and the radially polarized field, respectively.

In a next step we examine how the focal spot sizes can be reduced. From the scalar theory of diffraction it is well known that introducing an annular aperture reduces the spot size [7]. However, the side lobes become more pronounced, which leads to a reduced peak intensity. To transfer this concept to the vector treatment means that only those parts of the plane-wave spectrum having a large transverse component of the $\boldsymbol{k}$ vector are superposed in the focal region. In the mathematical treatment, this is considered by increasing the lower limit of the diffraction integral to a value $\theta_0 > 0$ [8]. In order to experimentally obtain the distribution of such an angular spectrum, an annular aperture has to be inserted in the front focal plane of the focussing system [9].

Surprisingly, the focal spot size of a linearly polarized beam increases slightly to a value of $0.330\,\lambda^2$ when inserting an annular aperture with an inner diameter of 90% of the lens diameter. This is an effect due to the vector character of the electric field. The shape of the focus is strongly deformed

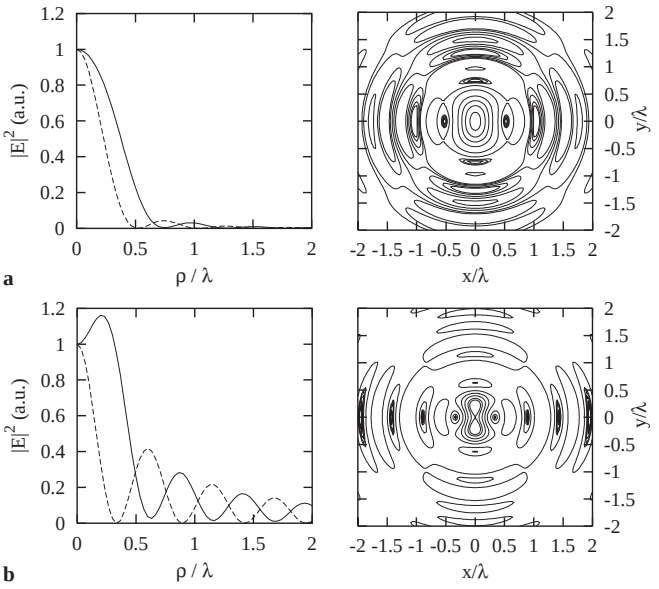

Fig. 3a,b. Comparison of the field distributions for linear polarization. Field distributions in the focal plane for **a** a beam with homogeneous intensity distribution and **b** a beam with annular field distribution. On the *right-hand side* a contour plot of the intensity distribution is depicted. The profiles along the direction of polarization (*solid line*) and the perpendicular direction (*dashed line*) are shown on the *left-hand side*. All curves have been calculated for NA = 1.0

and has the shape of a bone rather than the shape of an ellipse (Fig. 3b). In addition, the side lobes are very pronounced, reaching values of about 28% to 40% of the central intensity, depending on the direction of observation. In contrast, the spot size of the radially polarized field reduces considerably to $0.110\,\lambda^2$ when using the annular aperture. This is a factor of two smaller than in the case without the annular

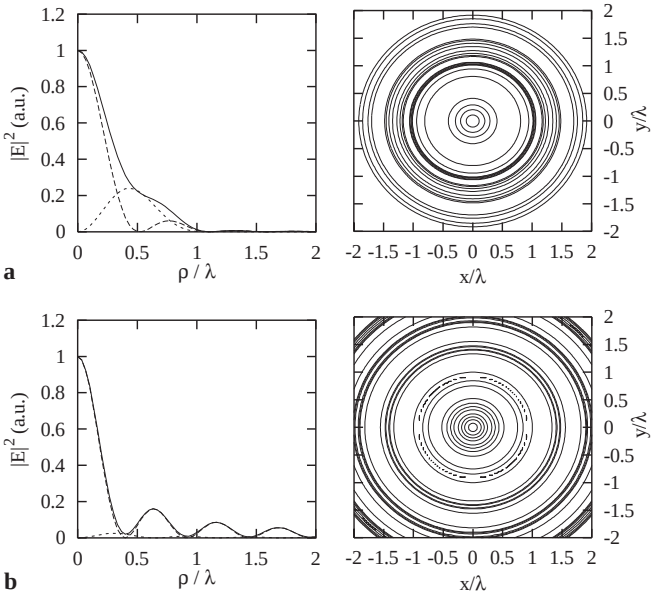

Fig. 4a,b. Profile of the rotationally symmetric focal field distribution of a radially polarized doughnut without **a** and with **b** an annular aperture. *Solid line*: total electrical intensity, *long dashed line*: longitudinal component, *dashed line*: transversal component of the electric field. All curves have been calculated for $NA = 1.0$

aperture and up to a factor of three smaller compared to the linearly polarized input field with an annular aperture. Moreover, the side lobes are less pronounced, i.e. the peak values of the side lobes' intensity are less than 18% of the intensity at the center (Fig. 4b). This is relevant for applications operating with a threshold criterion.

For high numerical apertures, the field distribution of the focussed radially polarized doughnut mode has a strong longitudinal component on the optical axis, while the transverse field vanishes. Off-axis, both longitudinal and transverse components are present. The focal spot size can be further reduced if there is a way to exploit only the narrow longitudinal component as shown by the long dashed lines in Fig. 4. Spot sizes of $0.160\,\lambda^2$ and $0.107\,\lambda^2$ can be reached with and without an annular aperture, respectively. These normal field components could be used exclusively, when having self-assembled monolayers of linear molecules all oriented normal to the surface. It is known that some molecules selectively react only to a light polarization oriented along the axis of the molecule [10]. Another method would be to use the boundary conditions of the electric field near the surface of a conductor. Normal, i.e. longitudinal electric-field components may exist right at the surface of the metal, while transverse components are reduced to zero by the induced surface currents. Therefore, a thin photosensitive layer on a metal substrate will experience only the normal electric-field components, even if the material itself is sensitive to all directions of polarization [3].

3 Experimental setup and measuring scheme

So far we have calculated the intensity distribution in the focus for high numerical aperture systems. The aim is now to measure the intensity distribution and the spot sizes for the various input fields experimentally. The experimental setup is based on the knife-edge method. The desired input-field distribution is focussed by a microscope objective onto specially designed *p-i-n* photodiodes. On the light-sensitive area of the diodes, rectangular and triangular gold pads with a thickness of about 100 nm were structured using electron-beam lithography. The orientation of the triangles on one of the diodes was rotated in steps of 10° relative to each other (Fig. 5). It is important that the edges of the gold pads are very sharp and straight to obtain high lateral resolution. These edges can be used as the knife edge, so that part of the focussed field can be blocked by the gold layer. In contrast to the conventional knife-edge method the transmitted light does not propagate any further, but it is detected directly by the photodiode. Thus effects of diffraction are minimized.

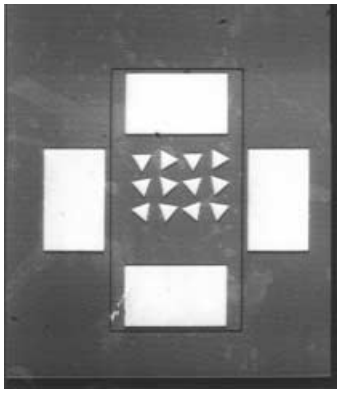

Fig. 5. SEM picture of the photodiode. The *rectangular structures* are the contact pads to tap the photocurrent; the *equilateral triangles* have a side length of 40 μm. The *triangles* provide the edges at different angles

The diode is mounted on an $x-y-z$ piezo-driven table. This allows us to move the diode and therefore the gold edges through the focus. The minimum step width was 13.4 nm. The gold structure partially blocks the beam in a plane perpendicular to the optical axis (Fig. 6). The photocurrent of the diode is proportional to the intensity that is incident on the light-sensitive area, which depends on the fraction of the beam blocked by one of the gold structures.

The photocurrent I_{Photo} depends on the displacement of the photodiode in the following way:

$$I_{\text{Photo}}(s, z_0) \propto \int_{-\infty}^{s} \int_{-\infty}^{\infty} I(x, y, z_0)\,\mathrm{d}x\,\mathrm{d}y, \tag{14}$$

where the intensity is measured in the plane at $z = z_0$, and x_0 is the position of the knife edge. A typical curve for the signal of the diode when it is moved through the focus is shown in Fig. 7a. I_{Photo} is equal to zero when the beam is completely blocked by the diode, and reaches a maximum value when the focal spot completely illuminates the photosensitive area. Figure 7b shows the first derivative of the measured curve

$$\frac{\partial I_{\text{Photo}}(s, z_0)}{\partial s} \propto \int_{-\infty}^{\infty} I(x = s, y, z_0)\,\mathrm{d}y, \tag{15}$$

which is proportional to the projection of the focal intensity distribution onto the translation axis along which the gold edge is moved through the focus. The task is to reconstruct the intensity distribution from the knowledge of the various projections.

Therefore, the gold edge is moved through the focus under N different angles which are equally spaced with a difference of $\Delta = \pi/N$ to each other. When the resulting curves are differentiated, one obtains the discrete Radon transformation $\mathcal{R}I$ of the intensity distribution in the focal plane. $\mathcal{R}I$ is therefore given as a set of N one-dimensional discrete functions $\{f_{n\Delta}\}(s)$. Now the discrete Radon back-projection [11]

$$[\mathcal{B}\{f_{n\Delta}\}](x, y) = \Delta \sum_{n=0}^{N-1} f_{n\Delta}(\underbrace{x \cos n\Delta + y \sin n\Delta}_{s}) \tag{16}$$

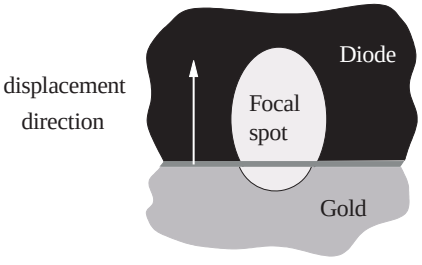

Fig. 6. Measurement scheme

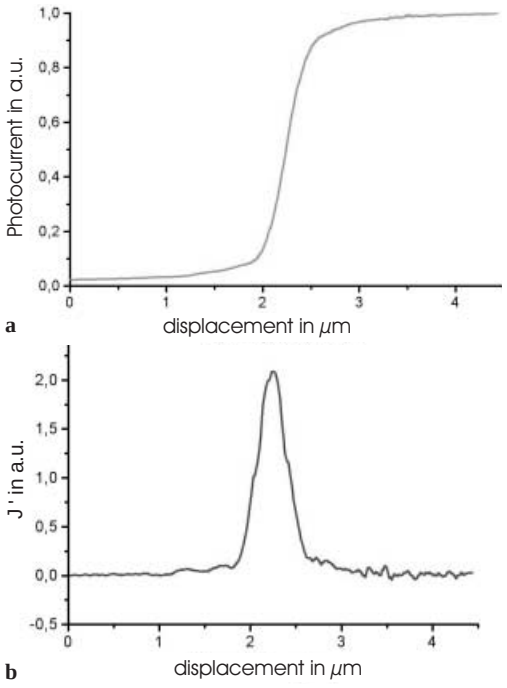

Fig. 7a,b. Photocurrent as a function of displacement (**a**). Differentiated signal of the photodiode (**b**)

can be applied to reconstruct the initial intensity distribution from the measured Radon transform

$$I(x, y) = \mathcal{B}\mathcal{F}^{-1}[|s| \cdot \mathcal{F}(\mathcal{R}I)](x, y). \tag{17}$$

Here '$\mathcal{F}$' and '$\mathcal{F}^{-1}$' denote the one-dimensional (inverse) Fourier transform with respect to the coordinate s. This technique is often used in tomography to reconstruct images from projections (see S. Rowland's article in [11]).

4 Experimental results

With this method we have performed a first test measurement. We measured the intensity distribution in the focal plane $z = 0$ for a homogeneous, linearly polarized input field that was focussed by a microscope objective with a numerical aperture of 0.8. We performed the measurement for 42 different angles by simultaneously rotating the microscope objective and the direction of polarization. The reconstructed intensity distribution in the focal plane is shown in Fig. 8a. The picture shows that coma effects due to aberrations of the objective are present. This can clearly be seen by the crescent-shaped structures along the x axis. In this measurement, the direction of polarization of the input field was oriented parallel to the y axis. There are also some underlying radially oriented structures in the reconstructed image, which are artefacts due to the limited number of projections for which measurements were made.

Figure 8b shows a comparison between the measured (reconstructed) intensity distribution in the center of the focus along the y axis, which is less affected by coma and the theoretical predictions (solid line).

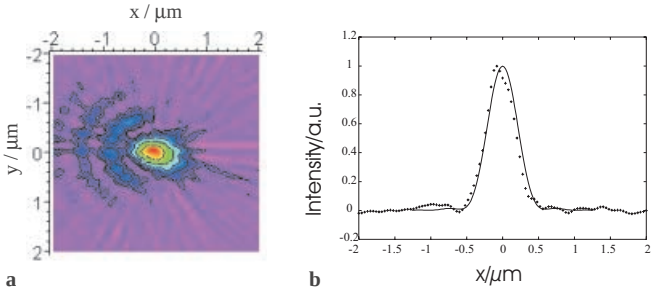

Fig. 8a,b. Reconstructed intensity distribution in the focal plane of a microscope objective where coma is present (**a**). Comparison of the reconstructed intensity distribution along the y-axis (+) with the theoretical prediction (−) (**b**)

5 Conclusion

For a focussing system with high numerical aperture, a radially polarized input field best matches the symmetry of the system and leads to a rotationally symmetric focal spot. In contrast to a linearly polarized input field, a strong field component parallel to the optical axis appears in the focal region. When an annular aperture is used, the spot size can be reduced by about a factor of two at the cost of increased side lobes. However, these side lobes are a factor of two to three smaller than the ones observed for a linearly polarized input field. An experimental setup was presented and demonstrated which is able to measure the three-dimensional intensity distribution in the vicinity of the focus. The setup allowed us to measure aberrations of the focussing microscope objective and is able to detect deviations in the shape of the focal field which are due to polarization effects. In a next step, the reduction of the spot size of a focussed radially polarized input field will be measured using an optimized setup with higher lateral resolution. Therefore the experimental setup will be improved by using an objective with higher numerical aperture and with a positioning system of higher spatial resolution. With this modified apparatus the focal deformation for linearly polarized light and the reduced spot size for radially polarized light will be measured.

References

1. B. Richards, E. Wolf: Proc. R. Soc. London, Ser. A **253**, 359 (1959)
2. J. Stamnes: *Waves in Focal Regions* (Adam Hilger, Bristol 1986) Chapt. 16
3. S. Quabis, R. Dorn, M. Eberler, O. Glöckl, G. Leuchs: Opt. Commun. **179**, 1 (2000)
4. H. J. Matthews, D. K. Hamilton, C. J. R. Sheppard: J. Mod. Opt. **36**, 233 (1989)
5. M. Müller, A. H. Buist, G. J. Brakenhoff, J. Squir: Opt. Commun. **138**, 16 (1997)
6. J.A. Arnaud, W.M. Hubbard, D.D. Mandeville, B. De la Claviere, E.A. Franke, J.M. Franke: Appl. Opt. **10**, 2775 (1971)
7. C. L. Matson: J. Opt. Soc. Am. A **15**, 33 (1998)
8. A. Yoshida, T. Asakura: Optik **40**, 322 (1974)
9. J. Durnin, J. J. Miceli, Jr., J. H. Eberly: Phys. Rev. Lett. **58**, 1499 (1987)
10. J. J. Macklin, J. K. Trautman, T. D. Harris, L. E. Brus: Science **272**, 255 (1996)
11. G. T. Herman (Ed.): *Image Reconstuction from Projections* (Springer, Berlin 1979)